A Novel Sustainable Flour Derived Hierarchical Nitrogen-Doped Porous Carbon/Polyaniline Electrode for Advanced Asymmetric Supercapacitors

*Pingping Yu, Zhiming Zhang, Lingxia Zheng, Feng Teng, Linfeng Hu, and Xiaosheng Fang**

Hierarchically porous nitrogen-doped carbon (HPC)/polyaniline (PANI) nanowire arrays nanocomposites are synthesized by a facile in situ polymerization. 3D interconnected honeycomb-like HPC was prepared by a cost-effective route via one-step carbonization using urea and alkali-treated wheat flour as carbon precursor with a high specific surface area (1294 $m^2 g^{-1}$). The specific capacitances of HPC and HPC/PANI (with a surface area of 923 $m^2 g^{-1}$) electrode are 383 and 1080 F g^{-1} in 1 M H_2SO_4, respectively. Furthermore, an asymmetric supercapacitor based on HPC/PANI as positive electrode and HPC as negative electrode is successfully assembled with a voltage window of 0–1.8 V in 1 M Na_2SO_4 aqueous electrolyte, exhibiting high specific capacitance (134 F g^{-1}), high energy density (60.3 Wh kg^{-1}) and power density (18 kW kg^{-1}), and excellent cycling stability (91.6% capacitance retention after 5000 cycles).

1. Introduction

Supercapacitors (SC) are one of the most promising energy sources for back-up power devices, cell phones, and hybrid electric vehicles, due to their superior power delivery, fast charge/discharge rate, and long cycle life (10^5 cycles).[1–3] However, the relative low energy densities (≤10 Wh kg^{-1}) of SCs severely limit their practical applications compared with rechargeable lithium batteries and fuel cells.[4,5] According to the equation $E = 1/2CV^2$,[6] the energy density (E) can be enhanced by increasing the device capacitance (C) using novel electrode materials or broadening the cell voltage (V) with different kinds of electrolytes. The organic or ionic liquid electrolytes provided wider potential windows (3–4 V) than aqueous electrolytes (1 V), but their poor ionic conductivity, high cost, and environmental pollution lead to unsatisfied practical application.[7] Therefore, designing asymmetric supercapacitors (ASCs) in aqueous electrolyte is an effective way to achieve a high energy density without sacrificing the specific power.[8–10]

The ASC devices generally consist of a cathode as the energy source and an anode as the power source. Activated carbon is the most widely used materials as anode for ASC because of high specific surface area (SSA), excellent chemical stability, moderate cost, and high conductivity. However, most of commercial porous activated carbon usually exhibit poor rate performance because of the insufficient ion diffusion within the micropores, which limits their energy density (5–8 Wh kg^{-1}) and power density.[11,12] The second-order structure of meso/macropores is essential to be induced. Thus, hierarchically porous carbons (HPCs) with rational distribution of interconnected macro, meso, and micropores are highly desired to replace currently used activated carbon. Recently, considerable research efforts have been devoted to develop various hierarchically porous carbon materials such as macro/mesoporous graphene framework,[13–15] porous graphene/carbon nanotube paper,[16] and nitrogen-doped porous carbon[17,18] as the electrodes. Nevertheless, the graphene, carbon nanotube (CNT), and nitrogen sources (e.g., polyaniline and polypyrrole) were used as precursors to prepare 3D porous carbon frameworks, which usually involved expensive/complex fabrication processes and were unfriendly to the environment, hindering the large area production for practical application. To obtain advanced electrode materials with optimized pore architectures in a facile and economic way, biomass as a biorenewable source can be directly carbonized as precursors to develop HPCs with high efficiency and ease of processability.[19] Moreover, the biomass carbon retains the framework of the pore-networks with high SAAs and desired pore size and shape. To date, many natural materials have been used to develop HPCs with excellent chemical capacitive performance via an easy, effective, and low-cost strategy, such as hemp,[20] willow catkins,[21,22] lignin,[23] wheat flour,[24] and rice bran,[25,26] In particular, ≈700 million tons of wheat are produced worldwide every year, while up to 14.4 million tons of wheat flour were wasted because of over processing in China, making them one of the best candidates for supercapacitors. Wheat flour consisting of starch (72%–80%) and protein (8–10%) can be well dispersed in distilled water to form suspension through vigorous stirring, and then form interconnected porous carbon

Dr. P. P. Yu, Z. M. Zhang, Dr. L. X. Zheng, Dr. F. Teng, Prof. L. F. Hu, Prof. X. S. Fang
Department of Materials Science
Fudan University
Shanghai 200433, China
E-mail: xshfang@fudan.edu.cn

DOI: 10.1002/aenm.201601111

of high SSA by carbonization process by using KOH as template and activating agent.[24] The interconnected ordered pores offer a large accessible surface area for increasing the charge accumulation. The HPC derived from wheat flour shows good electrochemical performance, and thus wasted wheat flour becomes a highly appreciated biomass carbon source.

Polyaniline (PANI) has become one of the attractive cathode candidate materials for supercapacitors due to its high electrical conductivity, ease of synthesis, low cost, and reversibility between redox states through doping/dedoping processes.[27–29] However, the swelling, shrinkage, and irreversible degradation of PANI during the charge/discharge process lead to poor stability.[30] One promising solution is to design ordered nanostructures of PANI, which has the advantages of good cycling stability, high specific capacitance, and excellent rate capability compared with randomly connected geometry.[31,32] Recently, PANI nanostructure has been employed in combination with carbonaceous materials (graphene and carbon nanotube)[33–35] and metal oxides (MnO_2, MoO_3, and Fe_2O_3) in designing asymmetric supercapacitors.[10,36,37] These studies have demonstrated that the synergistic effects between PANI and other active materials could improve conductivity of metal oxide or poor stability of PANI and enhance the specific capacitance of carbon materials, leading to high electrochemical performances.

In this study, we report a facile and cost-effective method to produce interconnected honeycomb-like hierarchically porous nitrogen-doped carbon (HPC) with narrow pore size distribution and high specific surface area by carbonization wheat flour. The urea, KOH, and wheat flour as the precursors were mixed to form gel solution and carbonized at 800 °C in nitrogen atmospheres as shown in **Scheme 1**. The as-prepared HPC with good electric conductivity demonstrate the synergistic effect of macro, meso, and microporosity (a high SSA up to 1294 $m^2 g^{-1}$) and consequently leading to a high-rate electrochemical performance with high specific capacitance (383 F g^{-1} at 1 A g^{-1}). Aligned PANI nanowires are grown on the surface of HPC by in situ polymerization (termed as HPC/PANI), which can enhance the specific capacitance and make high utilization of the continuous porous framework. Moreover, an asymmetric supercapacitor device in neutral electrolyte was assembled using HPC as the negative electrode and HPC/PANI as the positive electrode, respectively. It shows a maximum energy density of 60.3 Wh kg^{-1} (at a power density of 0.9 kW kg^{-1}) and power density of 18 kW kg^{-1} (at an energy density of 26 Wh kg^{-1}) at an operating voltage of 1.8 V in 1 M Na_2SO_4 aqueous electrolyte.

2. Results and Discussion

Figure 1a displays a low magnification scanning electron microscope (SEM) image revealing a honeycomb-like open sponge microstructure of HPC. The activation mechanism of wheat flour with KOH is followed by $6KOH + 2C \leftrightarrow 2K + 3H_2 + 2K_2CO_3$, then decomposition of K_2CO_3 and/or reaction of $K/K_2CO_3/CO_2$ with carbon.[4] SEM images of HPC0.5 and HPC1.5 (Figure S1, Supporting Information) also exhibit an analogous morphology as HPC, although the thickness of carbon wall decreases with increasing the mass ratio of wheat flour to KOH. The thickness of the carbon wall can be estimated in the range of 100 to 200 nm (Figure 1b). The KOH as template and activating agent can generate nanoscale pores in HPC. The meso/micropores and channels on the surface of carbon wall (Figure 1c) can be clearly seen by high resolution transmission electron microscope (TEM) images (Figure 1d). 3D architecture of HPC with interconnected macro, meso, and microporous structure will allow full access of the electrolyte to the active surface, shortening the diffusion pathways, and minimizing high-rate diffusional losses.[38] HPC can be used as a scaffold for loading active materials to enhance the specific capacitance. Three HPC/PANI composites (HPC/PANI3, HPC/PANI5, and HPC/PANI7) were prepared with tunable PANI nanostructures by controlling the concentration of aniline monomers as shown in **Figure 2**. Note that the original porous structure of HPC did not change after the loading of PANI via polymerization. The diameter of PANI increases as the aniline concentration increases. At a lower concentration, relative smaller and scattered PANI particles are produced for HPC/PANI3 (Figure 2a). While at higher concentration, denser and longer (100–200 nm) PANI nanowires randomly stack with each other for HPC/PANI7 due to the homogeneous nucleation process in the heterogeneous deposition process,[39] as shown in Figure 2d. In particular, with a moderate concentration of AN monomer, PANI nanowire arrays are uniformly grown on both the outer and internal wall surface of the HPC for sample HPC/PANI5 (Figure 2b,c). The average diameter of the nanowires is ≈20 nm and the length is ≈50 nm as observed from the TEM images (Figure 2e,f). The well-ordered PANI nanowire arrays grown on HPC are beneficial for delivering good capacitance and high-rate performance of electrode.

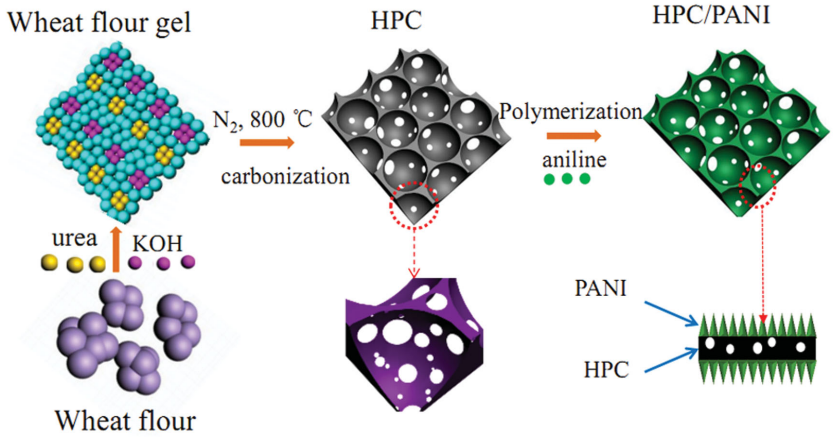

Scheme 1. Schematic illustration for the preparation of HPC/PANI composites.

Figure 3a presents the X-ray diffraction patterns of the HPC and HPC/PANI samples. The HPC shows two broader diffraction peaks at 25° and 43.7° corresponding to the (002) and (101) plane, respectively.[40] The typical diffraction peaks of PANI in the HPC/PANI are located at 25.3°, 20.3°, and 14.8°,

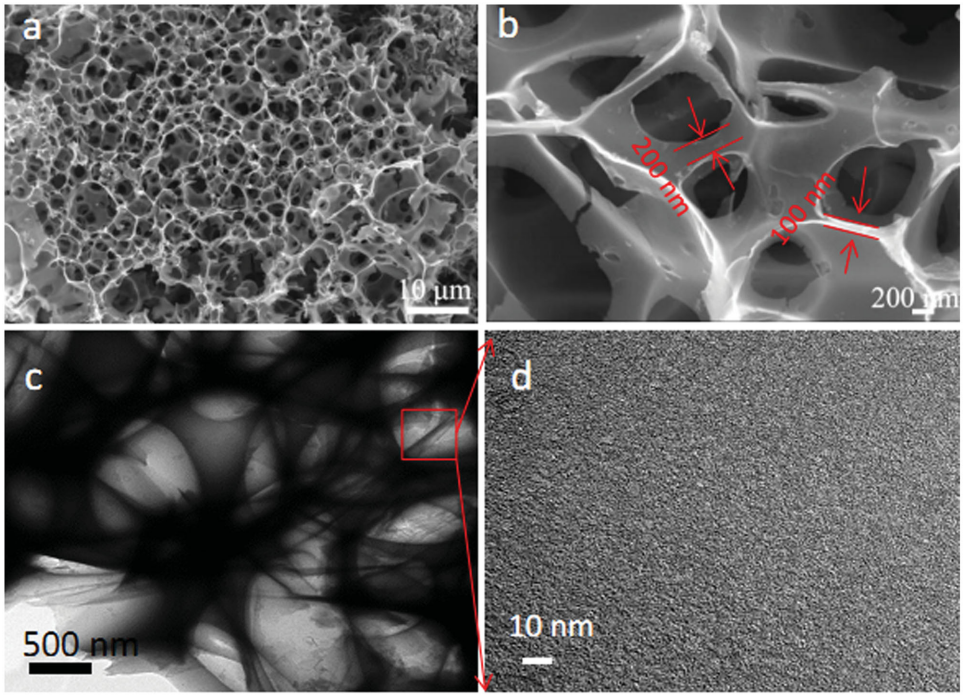

Figure 1. a,b) SEM images and c,d) TEM images of HPC.

corresponding to (200), (020), and (011) crystal planes of PANI in an emeraldine salt form, respectively.[32] The peak at 43.7° of HPC disappeared, indicating the complete coverage by PANI. Raman spectrum of HPC shows two typical bands at 1340 and 1590 cm^{-1} in Figure 3b, corresponding to the D (associated with defects) and G (related to graphitic carbon) bands, respectively.[20] Furthermore, the ratio of the integral intensity (I_D/I_G) is estimated to be 0.98, possessing the relatively highly graphitization and offering good electric conductivity, which is consistent with the XRD results. For HPC/PANI, the two signals of HPC are overlapped with characteristic peaks of PANI. The peaks at 1170, 1253, 1337, 1496, and 1590 cm^{-1} are attributed to the imine deformation, in-plane C—H bending, C—N·$^+$stretching vibration, C=N stretching vibration of quinoid ring, and C—C stretching of benzenoid ring, respectively.[41] In addition, X-ray photoelectron spectroscopy (XPS) measurements are performed to study the chemical identification of the heteroatoms in the HPC and HPC/PANI. The presence of C, N, and O elements can be seen in Figure 3c. This exhibits the partial conversion of N atoms (3.0 at%) from the urea and nitrogen atmosphere into the pyridinic-N (N-6, 398.6 eV), pyrrolic-N (N-5, 399.7 eV), and quaternary-N (N-Q, 401.1 eV) during the carbonization process (Figure S2a, Supporting Information).[40] The urea with high N content can react with oxygen-containing functional groups in wheat flour, thus acting as the nitrogen source to form the N-doped porous structure. The high resolution C 1s shows the presence of a C—N bond (285.8 eV) (Figure S2b, Supporting Information).[42] The N content of HPC/PANI is calculated to be 6.3 at%, high resolution of N 1s (Figure S2c, Supporting Information) can be deconvoluted into the forms of a quinoid imine (—N=), benzenoid amine (—NH—), and positively charged nitrogen atoms (—NH$^+$=), and with the corresponding peaks at 398.4, 399.8, and 401.6 eV, respectively.[28,33,43]

The highly porous structure of HPC and HPC/PANI composites was further determined by N_2 adsorption/desorption isothermal analysis (Figure 3d). All the samples show a I and IV type isothermal with a steep increase in N_2 adsorption at low pressure, indicating microporous carbon characteristics. The Brunauer–Emmett–Teller SSA of HPC is 1294 $m^2\ g^{-1}$, higher than that of HPC0.5 (1028 $m^2\ g^{-1}$) and HPC1.5 (1185 $m^2\ g^{-1}$) (Figure S3, Supporting Information). The obtained SSA values of HPC/PANI3 (1026 $m^2\ g^{-1}$), HPC/PANI5 (923 $m^2\ g^{-1}$), and HPC/PANI7 (704 $m^2\ g^{-1}$) are higher than the other reported carbon/PANI composites,[16,33,43] favorable for increasing the specific capacitance in supercapacitor applications. Narrow pore size distributions for all the samples are observed and mainly in the range of 1.0–4.0 nm (inset of Figure 3d). The decrease in the specific surface area with increasing PANI loading is mainly due to the pore-filling of PANI, which is confirmed by the negligible changed average pore size and the narrow pore size distribution.

The electrochemical properties of the HPC and HPC/PANI composites were conducted by cyclic voltammetry (CV), galvanostatic charge/discharge (GCD), and electrochemical impedance spectroscopy (EIS) in a three-electrode system in 1.0 M H_2SO_4 electrolyte. **Figure 4**a shows the CV curves of HPC and HPC/PANI electrodes at a scan rate of 50 mV s^{-1}. The CV curve of HPC shows nearly symmetric rectangular shape, indicating an ideal double-layer capacitor behavior. There is only a negligible change in the shape of the CV curve with increasing scan rates from 5 to 2000 mV s^{-1}, showing a good rate performance (Figure S4, Supporting Information) as a result of interconnected porous structure and effective nitrogen doping

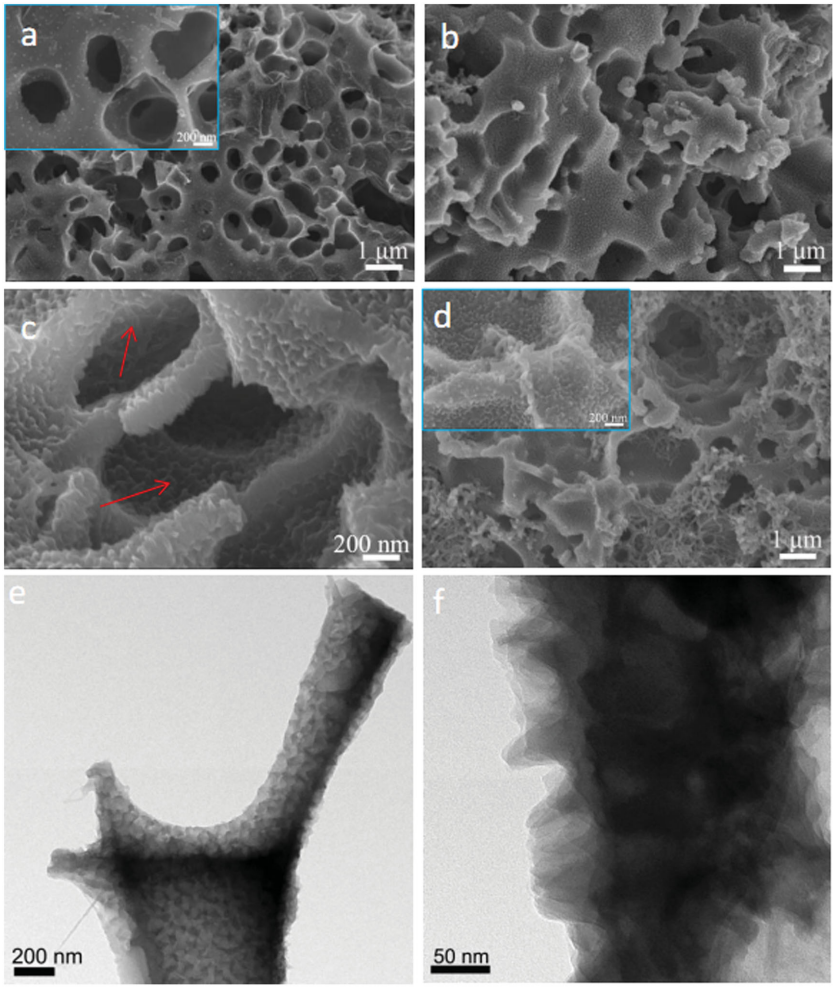

Figure 2. a) SEM images of HPC/PANI3, b,c) HPC/PANI5, and d) HPC/PANI7. TEM images of HPC/PANI5 at e) low and f) high resolution.

from urea. In the CV curves of HPC/PANI electrodes, the two pairs of peaks P_1/P_2 and P_5/P_6 are associated with the redox of PANI molecules (leucoemeraldine and pernigraniline species)[28] and the peaks P_3/P_4 are ascribed to benzoquinone/hydroquinone redox transitions.[39] The HPC/PANI5 shows larger integrated areas than that of the HPC, HPC/PANI3, and HPC/PANI7, revealing the highest specific capacitance. In addition, the enhancement of the C_{sp} is also confirmed by the GCD curves, as shown in Figure 4b. The C_{sp} of the HPC and HPC/PANI electrodes at various current densities is calculated from the discharge curves and is shown in Figure 4c. The C_{sp} of HPC is 383 F g^{-1} at a current density of 1 A g^{-1}, which is comparable to other previous reported porous carbon materials (**Table 1**). The 3D hierarchical porous structured HPC can provide interfacial transport, dispersion of active sites at different length scales of pores and largely shorten the diffusion path, in which interconnected macro/mesopores serve as ion-buffering reservoirs and ion-transport pathways, micropores enhance the electrical double layer.[19] Moreover, the abundant mesopores in the HPC can function effectively for charge storage at high current density. Compared with HPC/PANI3 (740 F g^{-1}) and HPC/PANI7 (752 F g^{-1}), the well-ordered HPC/PANI5 exhibits the highest specific capacitance of 1080 F g^{-1} at 1 A g^{-1}, which is much higher than other reported porous carbon/PANI composites (**Table 2**). This high capacitance mainly arises from the synergistic effect between interconnected porous HPC geometry and highly ordered PANI nanowire arrays based on the hierarchical nanostructure. The PANI nanowire arrays with narrow diameters provide shorter diffusion paths for the electrolyte ions, which can ensure the higher utilization of PANI. The interconnected macropores in the HPC/PANI5 can offer the highly conductive pathways and allow easy access of the electrolyte ions in the electrode during the rapid charge/discharge process. Additionally, HPC/PANI5 displays the same CV curves shape (Figure S5a, Supporting Information) and the similar charge/discharge plots (Figure S5b, Supporting Information) at various current densities, indicating a good rate capability.

Furthermore, EIS confirmed the fast ion diffusion process for HPC/PANI5 (Figure S5c, Supporting Information). Nyquist plots of all samples feature a vertical line at low-frequency region, indicating a nearly ideal capacitive behavior. At high-frequency region, the intercept with *X*-axis and diameter of semicircle represents the equivalent series resistance and interfacial charge transfer resistance (R_{ct}). The R_{ct} increases gradually with the increase of PANI content because of the low conductivity of PANI. The Nyquist plot of HPC/PANI5 exhibits no semicircle shape and the R_{ct} (0.87 Ω) is lower than HPC/PANI3 (0.89 Ω) and HPC/PANI7 (1.2 Ω), suggesting a good ion response of HPC/PANI5. Figure 4d shows the cycle stability of all the samples were conducted by GCD measurements at a current density of 1 A g^{-1}. The HPC electrode shows negligible capacitance degradation and keeps a high retention ratio of 95% after 5000 cycles, demonstrating a very stable electrode material. For the HPC/PANI electrodes, capacitance retentions of 80%, 88%, and 74% for HPC/PANI3, HPC/PANI5, and HPC/PANI7 are obtained, respectively. The improved electrochemical stability of HPC/PANI5 can be ascribed to three factors: highly interconnected 3D porous structure allows fasting ion diffusion and reduces the transport distance of electrolyte ions inside the micropores during the charge/discharge processes; strong π–π interaction between nitrogen-doped HPC and PANI prevents from the swelling and shrinkage caused by doping/dedoping; high surface area with nitrogen doping groups improves the wettability and provides more active sites for energy storage. The morphology of HPC/PANI5 electrode after 5000 cycles (Figure S6b, Supporting Information) mainly retains the array structure integrity, while the PANI nanowires are shortened to ≈40 nm in height due to the degradation under the long charge/discharge process. It

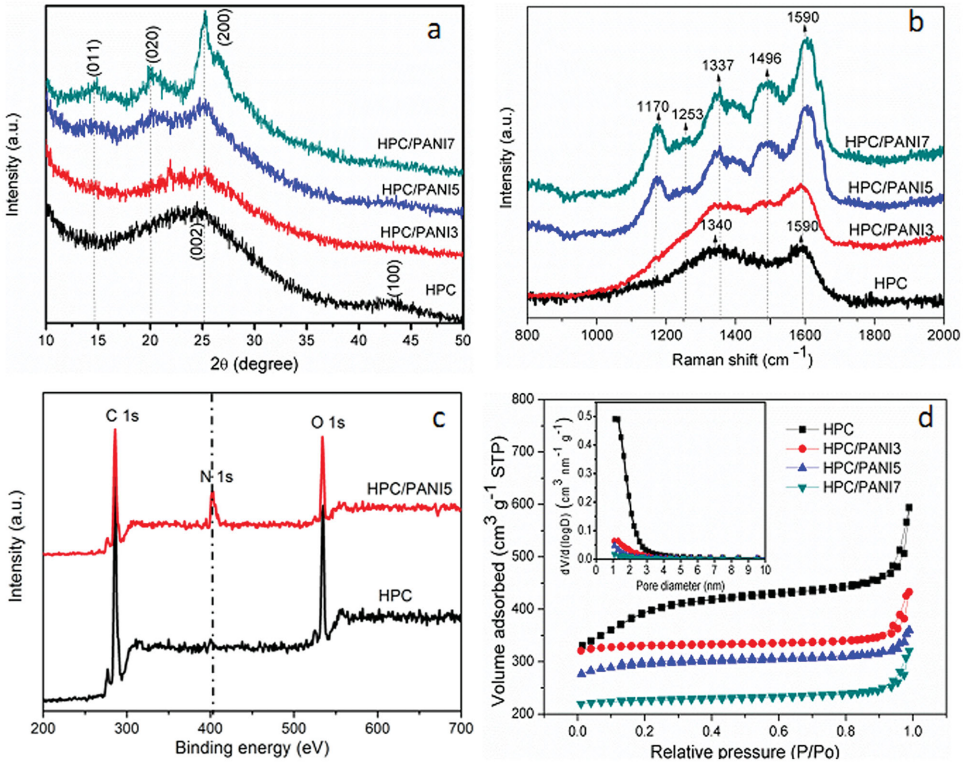

Figure 3. a) XRD patterns, b) Raman spectra, c) XPS analysis, and d) nitrogen adsorption/desorption isotherm (inset is pore size distribution) of HPC and HPC/PANI samples.

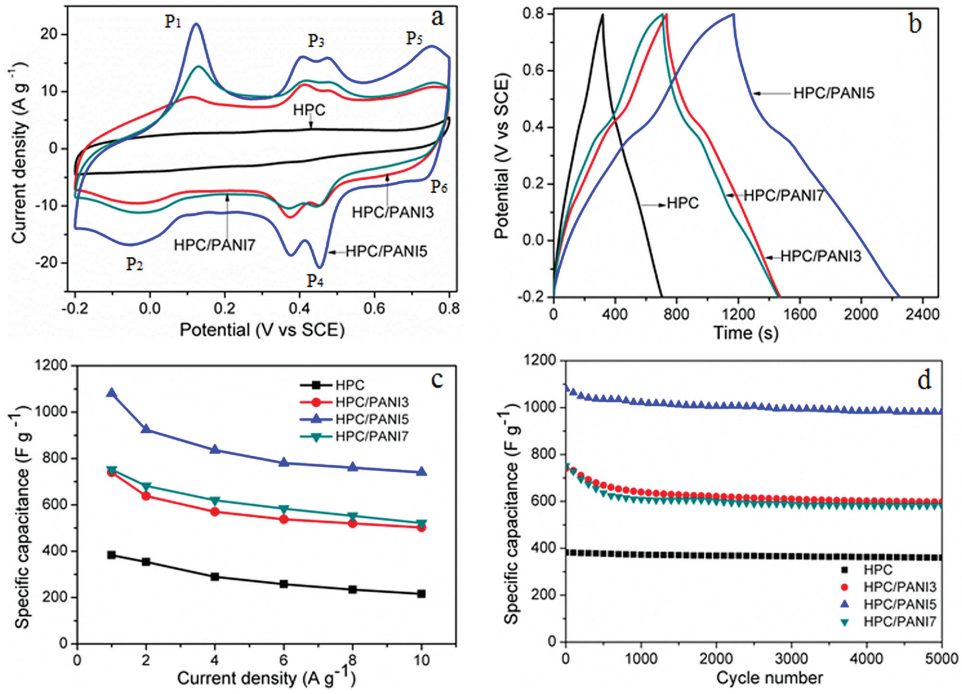

Figure 4. Electrochemical performances of HPC and HPC/PANI electrodes measured in a three-electrode system: a) Comparison of CV curves at a scan rate of 50 mV s^{-1}. b) Galvanostatic charge/discharge curves at 1 A g^{-1}. c) Specific capacitance as a function of current densities. d) Cycling performance at a current density of 1 A g^{-1}.

Table 1. Comparison of the specific capacitance for previously reported porous carbon materials in aqueous electrolyte.

Materials	C (F g^{-1})	El[a)]	R[b)]	M[c)]	Ref.
Seaweed derived HPC	425	1 M H_2SO_4	0.1 A g^{-1}	≈3.0–4.0	[12]
Wheat flour derived HPC	473 (N-doped)	6 M KOH	0.5 A g^{-1}	≈3.0	[24]
Willow catkin derived porous carbon sheets	298 (N-, S-doped)	6 M KOH	0.5 A g^{-1}	≈4.4	[22]
Tobacco derived carbon	287 (N-doped)	6 M KOH	0.5 A g^{-1}	≈6.0	[44]
Cotton fiber derived carbon aerogel	283	6 M KOH	1 A g^{-1}	≈1.0	[45]
Glucose derived carbon	322 (N-doped)	6 M KOH	1 A g^{-1}	NA	[42]
Pomelo peel derived carbon	342	6 M KOH	0.2 A g^{-1}	NA	[40]
Crumpled graphene	396	6 M KOH	0.5 A g^{-1}	≈1.0–2.0	[46]
Graphene hydrogel	425	2 M KOH	5 mv s^{-1}	≈1.0–1.5	[47]
HPC	383 (N-doped)	1 M H_2SO_4	1 A g^{-1}	≈2.0	This work

[a)]El: electrolyte type; [b)]R: current density or scan rate; [c)]M: mass loading (mg cm^{-2}).

can also be seen that the HPC/PANI3 (Figure S6a, Supporting Information) barely shows the PANI particles and HPC/PANI7 (Figure S6c, Supporting Information) exhibits the shrinkage and collapse of long PANI nanowires. Therefore, the optimized PANI nanowires in the hybrid electrode may improve the electrochemical performances.

In order to further evaluate the potential application of this hierarchical porous frame network electrode, ASC device based on HPC/PANI5 was tested in a two-electrode system using a safe aqueous 1 M Na_2SO_4 as an electrolyte. Here, the 3D interconnected porous nitrogen-doped HPC electrode with high-rate capability works as the negative electrode, and HPC/PANI5 electrode with high specific capacitance and fast charge transport property is selected as the positive electrode as shown in **Figure 5**a, which can simultaneously achieve high energy density and power density. The CV curves for HPC and HPC/PANI5 collected at different scan rates are shown in Figure S7a,c (Supporting Information) showing a good electrochemical response and reversibility. The specific capacitance of HPC/PANI5 is 634 F g^{-1} at 5 mV s^{-1}, while that of HPC is 128 F g^{-1}. Even at 100 mV s^{-1}, the capacitance still retains 85% and 60% retention of initial value for HPC and HPC/PANI5 electrodes (Figure S7b,d, Supporting Information). According to the CV test of HPC/PANI5 and HPC in a three-electrode system in 1 M Na_2SO_4 solution at 50 mV s^{-1} (Figure 5b), the corresponding specific capacitance is 422 and 109 F g^{-1}, respectively. To balance the charge storage in this asymmetric cell, the optimized mass ratio between HPC and PANI is calculated to be m(HPC/PANI5)/m(HPC) = 0.26. The stable potential window of 3D HPC is –1.0–0 V, while hierarchical porous HPC/PANI5 is stable between –0.2 and 0.8 V. The comparative CV curves of assembled HPC/PANI5// HPC ASC at different potential windows were measured at a scan rete of 50 mV s^{-1} to evaluate the optimized working potential (Figure 5c). The ASC device exhibits a stable voltage window at 0–1.8 V. When the potential is up to 2.0 V or higher, evolution of oxygen occurs.[36] The specific capacitance calculated from GCD plots at 1 A g^{-1} (Figure S8, Supporting Information) at different potential windows are displayed in Figure 5d. The value increases from 104 to 134 F g^{-1} as the potential range increase from 1.0 to 2.0 V. The GCD plot of ASC cell still maintains nearly symmetric even at 1.8 V, indicating the fast current response and small resistance. Therefore, the potential window of 1.8 V is chosen to further investigate the electrochemical performance for HPC/PANI5// HPC ASC cell.

HPC/PANI5//HPC ASC exhibits CV curves with the combination of both pseudocapacitive and double-layer capacitive behavior as shown in **Figure 6**a. The current increases as the scan rate increases, while its shape still remains even at a scan

Table 2. Comparison of the electrochemical performances for previous reported carbon/PANI composites in aqueous electrolyte.

Material	C (F g^{-1})	M[a)]	R[b)]	T[c)]	Cycle life	Ref.
Porous graphene/CNT/PANI paper	500	≈1.2	1 A g^{-1}	2-electrode GCD	85% (1000 cycles at 1 A g^{-1})	[16]
Graphene/PANI film	921	≈2.1	1 A g^{-1}	3-electrode GCD	85% (1000 cycles at 10 A g^{-1})	[27]
Graphene oxide/PANI/CNT	696	≈3.5	20 mV s^{-1}	3-electrode CV	89% (3000 cycles at 200 mV s^{-1})	[48]
Porous graphene/PANI film	740	NA	1 A g^{-1}	3-electrode GCD	87% (1000 cycles at 10 A g^{-1})	[43]
Macroporous carbon/PANI	662	≈2.5	1 A g^{-1}	3-electrode GCD	83% (7000 cycles at 2 A g^{-1})	[33]
Mesoporous carbon/PANI	803	≈5.0	0.1 A g^{-1}	2-electrode GCD	81% (1000 cycles at 4 A g^{-1})	[49]
Mesoporous carbon/PANI	900	≈5.0	0.5 A g^{-1}	3-electrode GCD	95% (3000 cycles at 5 A g^{-1})	[30]
HPC/PANI	1080	≈2.0	1 A g^{-1}	3-electrode GCD	88% (5000 cycles at 1 A g^{-1})	This work

[a)]M: mass loading (mg cm^{-2}); [b)]R: current density or scan rate; [c)]T: testing method.

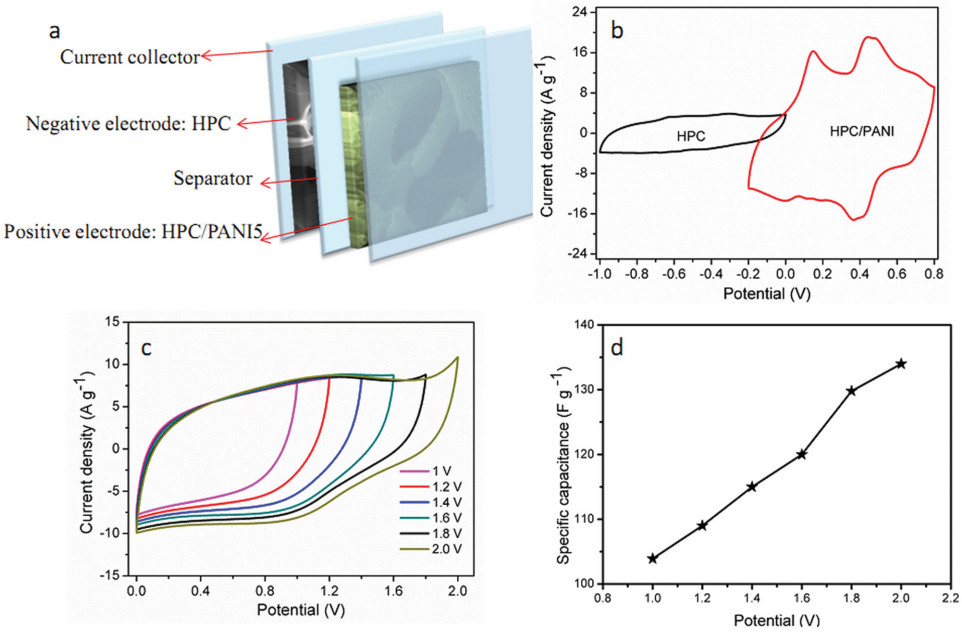

Figure 5. a) Schematic diagram of the structure of ASC device based on HPC and HPC/PANI5 electrodes. b) CV curves of the HPC and HPC/PANI5 electrodes collected at 50 mV s^{-1} in 1 M Na_2SO_4 aqueous solution in a three-electrode system. c) CV curves of HPC/PANI5//HPC ASC device measured at different potential window at 50 mV s^{-1}. d) Specific capacitance as a function of the various potential windows.

rate up to 200 mV s^{-1}. Figure 6b displays the GCD plots of the as-prepared ASC at various current densities in the potential window of 0–1.8 V. There is no obvious IR drop in the GCD plots indicating the small internal resistance (4 Ω) of ASC cell which can be observed in the Nyquist plot in Figure 6c. The symmetrical charge/discharge curves represents good capacitive characteristic. The C_{asy} is determined by the total weight of HPC negative electrode and HPC/PANI5 positive electrode.

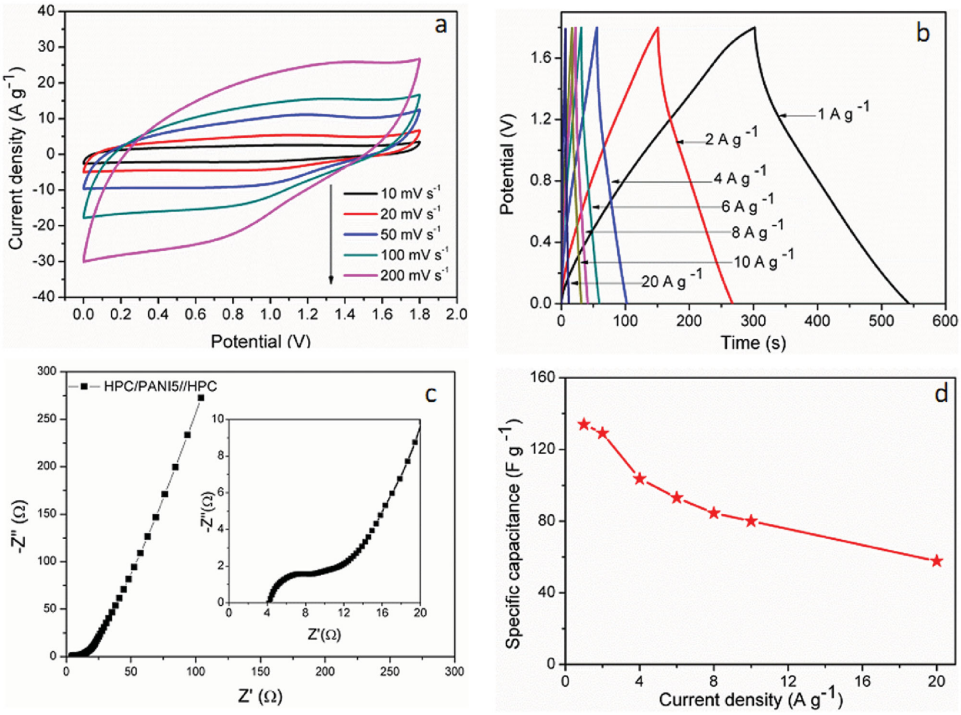

Figure 6. Electrochemical performance of HPC/PANI5//HPC ASC. a) CV curves at different scan rates. b) GCD curves at various current densities. c) Specific capacitance based on the total mass of the two electrodes versus current density. d) Nyquist plots with the inset showing the high-frequency region.

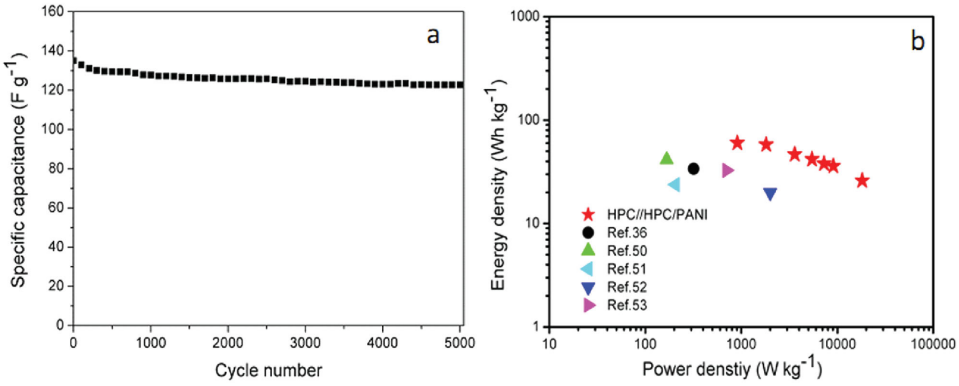

Figure 7. a) Cycling stability at a current density of 1 A g^{-1} and b) Ragone plots of HPC/PANI5//HPC ASC device.

The calculated gravimetric capacitances for our ASC cell (Figure 6d) is 134 F g^{-1} at a current density of 1 A g^{-1}, which is higher than other reported ASC based on PANI materials (61–107 F g^{-1}).[36,50,51] Even at a high current density of 20 A g^{-1}, the ASC device still has a high specific capacitance of 58 F g^{-1}, suggesting the improved mass transportation and high activated surface.

The cycling stability of the HPC/PANI5//HPC ASC is evaluated by the galvanostatic charge/discharge process in a voltage window of 0–1.8 V at a current density of 1 A g^{-1} for 5000 cycles (**Figure 7**a). The ASC device retains about 93% of the initial specific capacitance after the first 1000 cycles and a slight decrease in the capacitance to ≈91.6% retention after 5000 cycles, which is comparable to those of other ASC devices, including graphene/RuO_2//graphene/PANI ASC (70% retention after 2500 cycles),[9] graphene/CNT/PANI//porous graphene (91.4% retention after 2500 cycles),[50] PANI/MnO_2/carbon cloth//activated graphene (70% retention after 5000 cycles),[36] and CNT/PANI//CNT (91% retention after 5000 cycles).[35] Figure 7b shows the Ragone plots of (energy density vs power density) HPC/PANI5//HPC ASC. The maximum energy density operating at the 1.8 V voltage window is 60.3 Wh kg^{-1} at a power density of 0.9 kW kg^{-1} and still maintains 26 Wh kg^{-1} at a power density of 18 kW kg^{-1}. These values are superior to the previous reported ASC devices, such as PANI@MnO_2@carbon fiber//activated graphene (33.9 Wh kg^{-1}, 0.32 kW kg^{-1}),[36] graphene/CNT/PANI//graphene (41.5 Wh kg^{-1}, 0.17 kW kg^{-1}),[50] mesoporous carbon(CMK)/PANI//CMK (23.8 Wh kg^{-1}, 0.21 kW kg^{-1}),[51] activated carbon fiber/PANI//activated carbon (20 Wh kg^{-1}, 2 kW kg^{-1}),[52] and PANI nanotubes//CNT (32.7 Wh kg^{-1}, 0.7 kW kg^{-1}).[53] The special hierarchical porous structure with well-ordered PANI nanowire arrays uniformly grown on the very thin carbon wall surface facilitates the electrolyte ion into the whole electrode and ensures the high efficient charge storage. In addition, the 3D interconnected honeycomb-like porous framework with nitrogen doping can improve the surface wettability of the electrode and act as the mechanical support for PANI nanowires. The above results suggest that this low-cost and high-performance asymmetric supercapacitor can be a candidate for the energy storage device in future electronic applications.

3. Conclusion

The 3D interconnected honeycomb-like porous carbon with narrow pore distribution and high SSA was prepared by a cost-effective one-step carbonization route using wheat flour as carbon precursor. The nitrogen heteroatom-doped macroporous carbon frameworks (100–200 nm) enhance the surface wettability and hierarchical meso/micropores embedded surface provides a large accessible surface area and ions channels into the whole electrode. The well-ordered PANI nanowire arrays aligned on both internal and outer surface of the hierarchical porous HPC, showing a high specific capacitance of 1080 F g^{-1}. In addition, the assembled asymmetric supercapacitor based on HPC/PANI and HPC exhibits high energy density (60.3 Wh kg^{-1}) and power density (18 kW kg^{-1}), and a good cycling stability of 91.6% specific capacitance after 5000 cycles within the voltage window of 0–1.8 V in neutral aqueous solution. This special structure of HPC/PANI synthesized with facile and low-cost method shows a good electrochemical performance, making it a promising candidate in energy storage systems.

4. Experimental Section

Materials: The wheat flour used in the experiments was produced from a market in Fudan University. Hierarchically interconnected porous carbon was prepared by one-step carbonization using the mixture of wheat flour, urea, and KOH as the precursors. The mass ratio of wheat flour, urea, and KOH was 1:1:0.5, 1:1:1, and 1:1:1.5 (termed as HPC0.5, HPC, and HPC1.5, respectively). The mixture was vigorously stirred in 100 mL distilled water for 1 h, dried at 80 °C to evaporate the water and then heated at 800 °C (3 °C min^{-1}) for 2 h under nitrogen atmosphere. After that, the obtained carbon samples were thoroughly washed with 10% diluted HCl and deionized water. Finally, the samples were dried at 120 °C for 12 h before use.

HPC/PANI composites were synthesized by in situ polymerization. Aniline (AN, 45.65 µL) was added to 40 mL of 1 M H_2SO_4 aqueous solution and then stirred for 10 min to ensure complete dispersion. 100 mg HPC powders were added into the above solution and stirred for 2 h at 0 °C. Another 40 mL of 1 M H_2SO_4 cold aqueous solution containing ammonium peroxydisulfate (APS, 114.12 mg) was rapidly added and stirred for 5 min. The molar ratio of AN to APS was 1:1. The polymerization was carried out at 0 °C for 24 h, and the obtained HPC/PANI5 composite was washed with deionized water several times and

dried at 80 °C for 12 h in a vacuum oven. For comparison, the other composites with AN of 27.39 and 63.91 µL were fabricated under similar process, denoted as HPC/PANI3 and HPC/PANI7, respectively. The weight ratio of PANI in the HPC/PANI3, HPC/PANI5, and HPC/PANI7 composites is 5%, 16%, and 35%, respectively.

Material Characterization: The microstructures of HPC and HPC/PANI samples were conducted with field-emission scanning electron microscope (Zeiss Sigma) and TEM (TECNAI G^2 S-TWIN). X-ray diffraction patterns were collected on a Bruker D8-A25 diffractometer equipped with Cu Kα radiation (λ = 1.5405 Å). XPS was performed on a PHI 5000C ESCA system using a monochromatic Al X-ray source (97.9 W, 1486.6 eV). SSA and pore size were conducted by nitrogen adsorption–desorption method at 77 K on a Micromeritics Tristar ASAP 3000 analyzer. The Raman spectra were recorded on a LabRam-1B Raman spectroscope with He–Ne laser excitation at 632.8 nm and scanning for 50 s.

Electrochemical Measurements: All the electrochemical performances were measured on a CHI 660D electrochemical workstation at room temperature. The working slurry prepared by mixing the as-prepared samples (80 wt%), acetylene black (15 wt%), and polytetrafluoroethylene binder (5 wt%) was coated onto a titanium mesh (1 cm in diameter) and then dried at 100 °C overnight in a vacuum oven. A three-electrode system was used to measure the individual electrode in 1 M H_2SO_4 aqueous solution with Pt foil as the counter electrode and saturated calomel electrode (SCE) as the reference electrode, respectively. The ASC device fabricated by separating two electrodes with filter paper was tested in a two-electrode system using 1 M Na_2SO_4 as electrolytes, consisting of HPC as the negative electrode and HPC/PANI5 as positive electrode. The mass loading of active materials on the current collector is about 2 mg cm^{-2}.

The specific capacitance of a single electrode in the three-electrode cell was calculated according to

$$C = (\int IdV) / (\nu m \Delta V) \quad (1)$$

Gravimetric specific capacitance (F g^{-1}) was calculated from the galvanostatic charge/discharge curves by the following equation

$$C_{sp} = (I\Delta t) / (m\Delta V) \quad (2)$$

where I is the discharge current density (A), ν is the potential scanning rate (V s^{-1}), Δt is the discharge time (s), m is the mass of the electrode (g), and ΔV is the potential window (V).

The mass ratio of the positive and negative electrode was obtained based on the following equation

$$m_+ / m_- = (C_- V_-)/(C_+ V_+) \quad (3)$$

The specific capacitance of the whole ASC in two-electrode system was obtained by the equation

$$C_{asy} = (I\Delta t)/(M\Delta V) \quad (4)$$

where M ($M = m_+ + m_-$) is the total mass of the positive and negative electrodes. The energy density E (Wh kg^{-1}) and the power density P (W kg^{-1}) were calculated via the following equations

$$E = (C_{asy}\Delta V^2)/(2 \times 3.6) \quad (5)$$

$$P = 3600 \times E/\Delta t \quad (6)$$

Supporting Information

Supporting Information is available from the Wiley Online Library or from the author.

Acknowledgements

The authors thank Changzhou Almaden Company Limited to support this work. This work was financially supported by the Postdoctoral Science Foundation of China (Grant No. 2015M571487), the National Natural Science Foundation of China (Grant Nos. 51471051 and 51372040), the Science and Technology Commission of Shanghai Municipality (Grant No. 15520720700), the Shanghai Shu Guang Project (12SG01), the Shanghai Rising-Star Program (Grant No. 16QA1400700), and the Programs for Professor of Special Appointment (Eastern Scholar) at Shanghai Institutions of Higher Learning. Part of the experimental work was carried out in Fudan Nanofabrication Laboratory.

Received: May 27, 2016
Revised: June 12, 2016
Published online: July 25, 2016

[1] J. R. Miller, P. Simon, *Science* **2008**, *321*, 651.
[2] L. Yu, B. Y. Guan, W. Xiao, X. W. Lou, *Adv. Energy Mater.* **2015**, *5*, 1500981.
[3] S. X. Liu, L. F. Hu, X. J. Xu, A. A. Al-Ghamdi, X. S. Fang, *Small* **2015**, *11*, 4267.
[4] Y. Zhu, S. Murali, M. D. Stoller, K. J. Ganesh, W. Cai, P. J. Ferreira, A. Pirkle, R. M. Wallace, K. A. Cychosz, M. Thommes, D. Su, E. A. Stach, R. S. Ruoff, *Science* **2011**, *332*, 1537.
[5] J. M. Tarascon, M. Armand, *Nature* **2001**, *414*, 359.
[6] B. E. Conway, *Electrochemical Supercapacitors: Scientific Fundamentals and Technological Applications,* Plenum, New York **1999**.
[7] N. Kurra, R. Wang, H. N. Alshareef, *J. Mater. Chem. A.* **2015**, *3*, 7368.
[8] S. Peng, L. Li, H. B. Wu, S. Madhavi, X. W. Lou, *Adv. Energy Mater.* **2015**, *5*, 1401172.
[9] J. Liu, L. Zhang, H. B. Wu, J. Lin, Z. Shen, X. W. Lou, *Energy Environ. Sci.* **2014**, *7*, 3709.
[10] F. Su, C. K. Poh, J. S. Chen, G. Xu, D. Wang, Q. Li, J. Lin, X. W. Lou, *Energy Environ. Sci.* **2011**, *4*, 717.
[11] Z. S. Wu, W. Ren, D. W. Wang, F. Li, B. Liu, H. M. Cheng, *ACS Nano* **2010**, *4*, 5835.
[12] D. Kang, Q. Liu, J. Gu, Y. Su, W. Zhang, D. Zhang, *ACS Nano* **2015**, *9*, 11225.
[13] N. Gao, X. S. Fang, *Chem. Rev.* **2015**, *115*, 8294.
[14] L. L. Zhang, X. Zhao, M. D. Stoller, Y. Zhu, H. Ji, S. Murali, Y. Wu, S. Perales, B. Clevenger, R. S. Ruoff, *Nano Lett.* **2012**, *12*, 1806.
[15] S. C. Han, L. F. Hu, Z. Q. Liang, S. Wageh, A. A. Al-Ghamdi, Y. S. Chen, X. S. Fang, *Adv. Funct. Mater.* **2014**, *24*, 5719.
[16] W. Fan, Y.-E. Miao, L. Zhang, Y. Huang, T. Liu, *RSC Adv.* **2015**, *5*, 31064.
[17] J. Han, G. Xu, B. Ding, J. Pan, H. Dou, D. R. MacFarlane, *J. Mater. Chem. A* **2014**, *2*, 5352.
[18] X. Ning, W. Zhong, S. Li, Y. Wang, W. Yang, *J. Mater. Chem. A* **2014**, *2*, 8859.
[19] S. Dutta, A. Bhaumik, K. C.-W. Wu, *Energy Environ. Sci.* **2014**, *7*, 3574.
[20] H. Wang, Z. W. Xu, A. Kohandehghan, Z. Li, K. Cui, X. H. Tan, T. J. Stephenson, C. K. King'ondu, C. M. B. Holt, B. C. Olsen, J. K. Tak, D. Harfield, A. O. Anyia, D. Mitlin, *ACS Nano* **2013**, *7*, 5131.
[21] L. J. Xie, G. H. Sun, F.Y. Su, X. Q. Guo, Q. Q. Kong, X. M. Li, X. H. Huang, L. Wan, W. Song, K. X. Li, C. X. Lv, C. M. Chen, *J. Mater. Chem. A* **2016**, *4*, 1637.
[22] Y. Li, G. Wang, T. Wei, Z. Fan, P. Yan, *Nano Energy* **2016**, *19*, 165.
[23] H. Li, D. Yuan, C. Tang, S. Wang, J. Sun, Z. Li, T. Tang, F. Wang, H. Gong, C. He, *Carbon* **2016**, *100*, 151.

[24] X. Wu, L. Jiang, C. Long, Z. Fan, *Nano Energy* **2015**, *13*, 527.
[25] J. Hou, C. Cao, X. Ma, F. Idrees, B. Xu, X. Hao, W. Lin, *Sci. Rep.* **2014**, *4*, 7260.
[26] N. Liu, K. Huo, M. T. McDowell, J. Zhao, Y. Cui, *Sci. Rep.* **2013**, *3*, 1919.
[27] N. Hu, L. Zhang, C. Yang, J. Zhao, Z. Yang, H. Wei, H. Liao, Z. Feng, A. Fisher, Y. Zhang, Z. J. Xu, *Sci. Rep.* **2016**, *6*, 19777.
[28] B. Song, L. Li, Z. Lin, Z. K. Wu, K. S. Moon, C. P. Wong, *Nano Energy* **2015**, *16*, 470.
[29] P. J. Hung, K. H. Chang, Y. F. Lee, C. C. Hu, K. M. Lin, *Electrochim. Acta* **2010**, *55*, 6015.
[30] Y. G. Wang, H. Q. Li, Y. Y. Xia, *Adv. Mater.* **2006**, *18*, 2619.
[31] Y. Li, X. Zhao, P. Yu, Q. Zhang, *Langmuir* **2012**, *29*, 493.
[32] P. P. Yu, Y. Z. Li, X. Zhao, L. H. Wu, Q. H. Zhang, *Synth. Met.* **2013**, *185*, 89.
[33] J. P. Li, Y. Q. Ren, Z. H. Ren, S. G. Wang, Y. J. Qiu, J. Yu, *J. Mater. Chem. A* **2015**, *3*, 23307.
[34] K. V. Sankar, R. K. Selvan, *J. Power Sources* **2015**, *275*, 399.
[35] M. Khalid, M. A. Tumelero, A. A. Pasa, *RSC Adv.* **2015**, *5*, 62033.
[36] X. Zhao, C. Chen, Z. Huang, L. Jin, J. Zhang, Y. Li, L. Zhang, Q. Zhang, *RSC Adv.* **2015**, *5*, 66311.
[37] F. Jiang, W. Li, R. Zou, Q. Liu, K. Xu, L. An, J. Hu, *Nano Energy* **2014**, *7*, 72.
[38] J. Ding, H. L. Wang, Z. Li, K. Cui, D. Karpuzov, X. H. Tan, A. Kohandehghan, D. Mitlin, *Energy Environ. Sci.* **2015**, *8*, 941.
[39] P. Yu, X. Zhao, Z. Huang, Y. Li, Q. Zhang, *J. Mater. Chem. A* **2014**, *2*, 14413.
[40] Q. Liang, L. Ye, Z. H. Huang, Q. Xu, Y. Bai, F. Kang, Q. H. Yang, *Nanoscale* **2014**, *6*, 13831.
[41] D. Li, Y. Li, Y. Feng, W. Hu, W. Feng, *J. Mater. Chem. A* **2015**, *3*, 2135.
[42] J. Y. Liang, C. C. Wang, S. Y. Lu, *J. Mater. Chem. A* **2015**, *3*, 24453.
[43] S. Wang, L. Ma, M. Gan, S. Fu, W. Dai, T. Zhou, X. Sun, H. Wang, H. Wang, *J. Power Sources* **2015**, *299*, 347.
[44] Y. Q. Zhao, M. Lu, P. Y. Tao, Y. J. Zhang, X. T. Gong, Z. Yang, G. Q. Zhang, H. L. Li, *J. Power Sources* **2016**, *307*, 391.
[45] P. Cheng, T. Li, H. Yu, L. Zhi, Z. Liu, Z. Lei, *J. Phys. Chem. C* **2016**, *120*, 2079.
[46] J. Y. Lee, K. H. Lee, Y. J. Kim, J. S. Ha, S. S. Lee, J. G. Son, *Adv. Funct. Mater.* **2015**, *25*, 3606.
[47] R. Wang, C. Xu, J. M. Lee, *Nano Energy* **2016**, *19*, 210.
[48] M. Hao, Y. Chen, W. Xiong, L. Zhang, L. Wu, Y. Fu, T. Mei, J. Wang, J. Li, X. Wang, *Electrochim. Acta* **2016**, *191*, 165.
[49] Z. Lei, X. Sun, H. Wang, Z. Liu, X. S. Zhao, *ACS Appl. Mater. Interfaces* **2013**, *5*, 7501.
[50] J. Shen, C. Yang, X. Li, G. Wang, *ACS Appl. Mater. Interfaces* **2013**, *5*, 8467.
[51] J. J. Cai, L. B. Kong, J. Zhang, Y. C. Luo, L. Kang, *Chin. Chem. Lett.* **2010**, *21*, 1509.
[52] D. Salinas-Torres, J. M. Sieben, D. Lozano-Castelló, D. Cazorla-Amorós, E. Morallón, *Electrochim. Acta* **2013**, *89*, 326.
[53] N. An, Y. F. An, Z. G. Hu, Y. D. Zhang, Y. Y. Yang, Z. Q. Lei, *RSC Adv.* **2015**, *5*, 63624.